

Article

Effect of Temperature on the Functionalization Process of Structural Self-Healing Epoxy Resin

Luigi Vertuccio¹, Elisa Calabrese² , Marialuigia Raimondo² , Michelina Catauro¹ , Andrea Sorrentino³ , Carlo Naddeo² , Raffaele Longo²  and Liberata Guadagno^{2,*} 

- ¹ Department of Engineering, University of Campania “Luigi Vanvitelli”, Via Roma 29, 81031 Aversa, Italy; luigi.vertuccio@unicampania.it (L.V.); michelina.catauro@unicampania.it (M.C.)
- ² Department of Industrial Engineering, University of Salerno, Via Giovanni Paolo II, 132, 84084 Fisciano, Italy; elicalabrese@unisa.it (E.C.); mraimondo@unisa.it (M.R.); cnaddeo@unisa.it (C.N.); rlongo@unisa.it (R.L.)
- ³ Institute for Polymers, Composites, and Biomaterials (IPCB-CNR), Via Previati n. 1/E, 23900 Lecco, Italy; andrea.sorrentino@cnr.it
- * Correspondence: lguadagno@unisa.it

Abstract: This work deals with developing a self-healing resin designed for aeronautical and aerospace applications. The bifunctional epoxy precursor was suitably functionalized to enhance its toughness to realize good compatibilization with a rubber phase dispersed in the hosting epoxy resin. Subsequently, the resulting mixture was loaded with healing molecules. The effect of the temperature on the epoxy precursor’s functionalization process was deeply studied. Fourier transform infrared (FT-IR) spectroscopy and dynamic mechanical analyses (DMA) evidenced that the highest temperature (160 °C) allows for obtaining a bigger amount of rubber phase bonded to the matrix. Elastomeric domains of dimensions lower than 500–600 nanometers were found well distributed in the matrix. Self-healing efficiency evaluated with the tapered double cantilever beam (TDCB) method evidenced a healing efficiency for the system functionalized at 160 °C higher than 69% for all the explored fillers. The highest value was detected for the sample with DBA, for which 88% was found. The healing efficiency of the same sample functionalized at 120 °C was found to decrease to the value of 52%. These results evidence the relevant role of the amount and distribution of rubber domains into the resin for improving the resin’s dynamic properties. The adopted strategy allows for optimizing the self-healing performance.

Keywords: self-healing efficiency; functionalization reaction; epoxy resin; mechanical properties



Citation: Vertuccio, L.; Calabrese, E.; Raimondo, M.; Catauro, M.; Sorrentino, A.; Naddeo, C.; Longo, R.; Guadagno, L. Effect of Temperature on the Functionalization Process of Structural Self-Healing Epoxy Resin. *Aerospace* **2023**, *10*, 476. <https://doi.org/10.3390/aerospace10050476>

Academic Editor: Khamis Essa

Received: 12 March 2023

Revised: 11 May 2023

Accepted: 16 May 2023

Published: 18 May 2023



Copyright: © 2023 by the authors. Licensee MDPI, Basel, Switzerland. This article is an open access article distributed under the terms and conditions of the Creative Commons Attribution (CC BY) license (<https://creativecommons.org/licenses/by/4.0/>).

1. Introduction

Self-healing materials can repair themselves and recover integrity using the resources inherently available or healing mechanisms activated during microfractures. The auto-repair process can be autonomic or externally assisted, but it is always triggered by damage to the material. The integration of the self-healing functionality in thermosetting resins is driven by the need to reduce the environmental impact and the speed of resource depletion. This can be achieved by consistently reducing starting materials (primary resources) and, as a consequence, energy consumption and CO₂ emissions into the atmosphere. Together with the atmosphere decarbonization contribution, the possibility to auto-repair polymeric materials significantly impacts the speed reduction of producing end-of-life plastic wastes. A strong impact on cost reduction is also expected, deriving from the longer life of materials and reduced demand for resources necessary to produce new ones. Ultimately, all this would translate into a high environmental impact reduction and energy sustainability promotion. Furthermore, together with the reduction of maintenance operations on composite components, the possibility to guarantee the structural integrity of components in spaces inaccessible for maintenance operations is strongly felt in aeronautics and aerospace.

The studies carried out until now on auto-repair polymeric materials have resulted in innumerable healing designs that recently are focused on complex systems capable of supporting multiple cycles [1–10].

Self-healing polymers can be divided as extrinsic and intrinsic [8,11]. Extrinsic polymers are based on auto-repair processes depending on external healing agents in micro/nano vessels (generally in the form of microcapsules or vascular channels). The healing agents are released to seal the damaged regions.

Capsule-based self-healing systems retain the healing agent in microcapsules. When the damage occurs and propagates in the material, the microcapsules are cracked and the self-healing mechanism is triggered, leading to a local healing event. The main systems involve the encapsulation of a liquid healing agent and the dispersion of a catalyst, active in the ring-opening metathesis polymerization (ROMP), inside the polymeric matrix [12–15]. This strategy was also used to impart self-healing features to an epoxy resin modified with CTBN rubber for application as an adhesive by Henghua Jin et al. [16]. In particular, the authors developed a toughened epoxy adhesive where self-healing is achieved via embedded microcapsules containing dicyclopentadiene monomer and Grubbs' catalyst. Vascular self-healing materials sequester the healing agent in one, two, or three-dimensional networks consisting of capillaries or hollow channels [17–20].

Intrinsic self-healing polymers are those in which the reversible bonds (dynamic covalent and noncovalent bonds) active in the material can restore the integrity of the polymer after a damage event [11,21].

Therefore, these self-healing polymers are based on the inherent reversibility of bonding of the matrix polymer. For this typology of self-healing polymers, healing events can be achieved by reversible covalent reactions [22–33], the presence of a dispersed meltable thermoplastic phase [34,35], ionic coupling [36–39], via molecular diffusion [40–42] or hydrogen bonding [36–39,43,44]. The intrinsic self-healing materials are less complex than capsule-based and vascular self-healing materials, avoiding the problems related to healing-agent integration, compatibility, catalyst stability, etc. [13,45]. However, most self-healing intrinsic systems have mechanical and chemical properties incompatible with those required by structural applications.

Thermosetting resins, with their combination of thermal stability, performance, and chemical resistance, are extensively used in industry. However, integrating self-healing functionality into these materials is very difficult due to their irreversible network structure and low chain mobility, which impede the chain flow necessary for the common self-healing process [46].

To address this challenge, different approaches have been experimented in literature [46]. In previous works the authors have proposed an intrinsic self-healing system consisting of an epoxy resin covalently modified by a rubber phase containing self-healing fillers [47,48]. The presence of the elastomer has allowed reducing the rigidity of the epoxy chains and promoting the activation of an auto-repair mechanism based on hydrogen bonding interactions. Furthermore, rubber-toughened thermosetting resins manifest several advantages compared with the unmodified resin. Ricciardi et al. [49] used nitrile rubber to toughen glass fiber reinforced EP composites. They found that the modified composites showed smaller delamination, although the absorbed energy was the same and the load was higher. Karger-Kocsis and Friedrich analyzed fatigue crack propagation of carboxyl-terminated acrylonitrile-butadiene rubber (CTBN) and silicon rubber (SI) modified Epoxy resin [50,51]. The incorporation of CTBN and/or SI dispersion in the EP matrix improved the resistance to fatigue crack propagation.

In order to not significantly alter the mechanical properties of the resin, intended for structural applications (such as aerospace or automotive fields), different fillers or nano-fillers have been solubilized/dispersed into the epoxy matrix [47,48].

This work focuses on the effect of the curing temperature of a rubber-toughened bifunctional epoxy resin filled with self-healing molecules to impart an auto-repair function to the resin. FT/IR analysis and dynamic mechanical analyses (DMA) were used to study

the functionalization of the epoxy precursor and to estimate the amount of the elastomeric phase bonded to the epoxy precursor for different temperatures of functionalization. A more significant amount of rubber phase bonded to the matrix was found for the functionalization performed at the higher temperature of 160 °C compared to that conducted at 120 °C. Thermogravimetric analysis was employed to evaluate the beginning of the degradation temperature for all the formulated systems. Self-healing tests performed through the tapered double cantilever beam (TDCB) evidence a higher healing efficiency for the selected system functionalized at 160 °C, containing the healing molecules. A synergistic effect between the interactions determined by the active self-healing fillers and those due to the presence of elastomeric domains bonded to the epoxy precursor has been hypothesized.

2. Materials and Methods

2.1. Materials

The formulated samples are composed by a hosting toughened epoxy matrix consisting of the precursor “3,4-Epoxy cyclohexylmethyl-3',4'-epoxy cyclohexane carboxylate” (ECC—Empirical Formula $C_{14}H_{20}O_4$) (see the chemical structure in Figure 1a) (Gurit Holding, Wattwil, Switzerland) and the hardener agent “Methylhexahydrophthalic anhydride” (MHHPA—Empirical Formula $C_9H_{12}O_3$) (see the chemical structure in Figure 1b) (Gurit Holding, Wattwil, Switzerland), both used in a ratio 1:1. As toughening agent (5 wt% with respect to the total mixture) the liquid rubber Carboxyl-Terminated Butadiene Acrylonitrile Copolymer was employed (R, see the chemical structure in Figure 1c) supplied by Hycar-Reactive Liquid Polymers, with $M_n = 3600$, containing terminal carboxy groups (COOH content of 0.67×10^{-3} equiv/g of CTBN and 18 w/w% of CN). The compound triphenyl phosphine (PPh_3 , Merck KGaA, Darmstadt, Germany), added in an amount of 10 wt%, was employed as a catalyst to promote the functionalization reaction of the epoxy precursor (ECC).

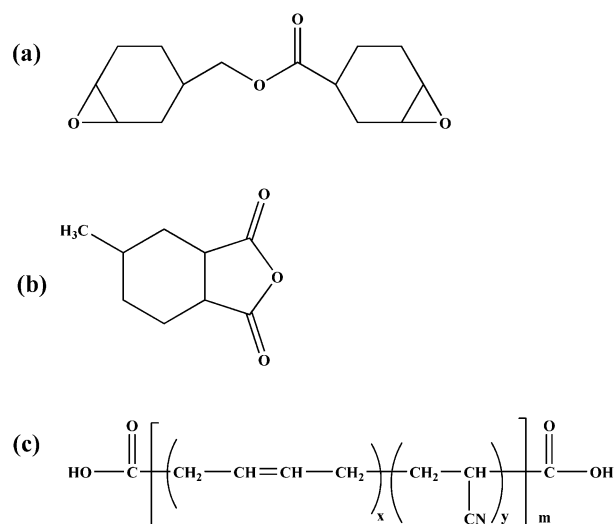


Figure 1. Chemical structures of the: (a) epoxy precursor (ECC); (b) hardener (MHHPA); (c) liquid rubber (R).

Table 1 shows the amount in grams of each component to prepare 23.58 g of a complete mixture Ep-R-120 or Ep-R-160.

Considering the chosen composition, the first Nucleophilic attack by triphenylphosphine (see reaction scheme in Section 3.1.1 FT-IR Analysis) opens 9.15×10^{-3} mol of oxirane rings, leaving 7.0×10^{-2} mol of oxirane rings still unreacted (not opened). After the first Nucleophilic attack of PPh_3 , the unreacted oxirane rings represent 88% of the initially available rings. The moles of the terminal carboxylic groups are 0.804×10^{-3} . This amount (in mol) is slightly defective compared with the opened oxirane rings (9.15×10^{-3} mol). This choice has been made to avoid big domains of elastomeric phase in the resin (as highlighted later

through SEM investigation). The question of the dimensions of the rubber domains has been a nontrivial issue that has been addressed before choosing the chemical composition of the epoxy mixture. Based on data already reported in literature [52] and authors' experience, a lower amount of triphenylphosphine (or a higher amount of rubber phase with respect to the same amount of PPh₃) determines a higher dimension of the elastomer domains, causing local inhomogeneity in the order of hundreds or units of microns with consistent local inhomogeneity.

Table 1. Amount in grams of each component to prepare 23.58 g of a complete mixture Ep-R-120 or Ep-R-160.

Component	Ep-R-120/Ep-R-160
ECC [g]	10.0
CTBN [g]	1.2
PPh ₃ [g]	2.4
MHHPA [g]	10.0

The self-healing fillers 1,3-Dimethylbarbituric acid (DBA), 2-Thiohydantoin (T), and Murexide (M) (all purchased from Merck KGaA, Darmstadt, Germany) have been added in a percentage of 0.42 wt% (see Figure 2). The ability of these fillers to activate self-healing mechanisms, based on hydrogen bonding interactions, was already demonstrated in previous work with a nano-charged resin based on a tetrafunctional epoxy precursor hardened with 4,4-diamino diphenyl sulfone [47]. The matrix was loaded with conductive nanofillers, and the healing efficiency was evaluated for the formulation with 0.5% by weight of carbon nanotubes to confer functional properties to the resin. Generally, the presence of conductive fillers confers many functional properties to the hosting polymeric matrix [53–55]. In particular, electrically conductive fillers such as CNTs, graphene-based nanoparticles, or expanded graphite have been dispersed in optimized epoxy resins to impart them self-sensing for the damage monitoring [56,57] or for activating the anti/de-icing function through the joule effect [58–60], or to make possible energy saving curing processes (electro-curing processes) of resins/composites [61], and for enhancing adhesive properties [62].

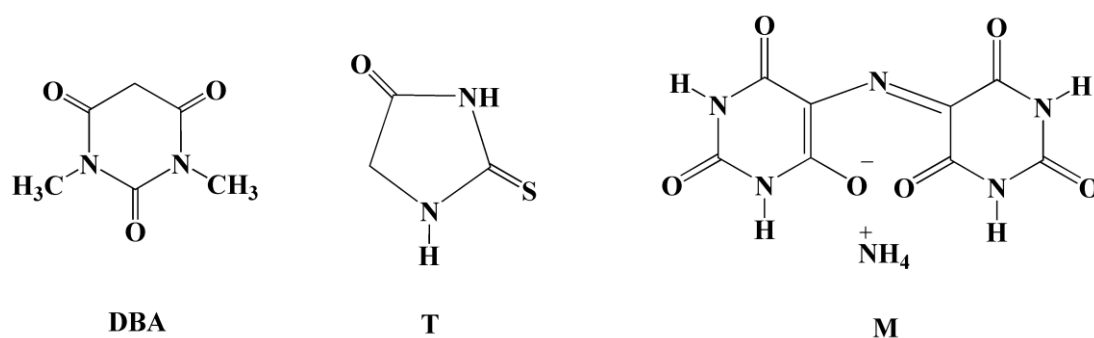


Figure 2. Chemical structure of molecules acting as self-healing filler.

2.2. Formulation of Epoxy Samples

2.2.1. Functionalized Epoxy Precursor

The functionalized precursor liquid blends ECC-R-120 and ECC-R-160 were composed of the epoxy precursor covalently modified with the rubber phase.

The two blends were obtained by mixing, under mechanical stirring, the epoxy precursor ECC, the elastomer R, and the catalyst PPh₃ for a time of 15 h, at temperatures of 120 and 160 °C, respectively.

2.2.2. Functionalized Epoxy Samples

The cured epoxy samples Ep-R-120 and Ep-R-160 were composed of the precursor functionalized at the temperature of 120 and 160 °C, respectively. They were obtained by mixing by magnetic stirring for 20 min at room temperature, the hardener MHHPA and the functionalized precursor (ECC-R-120 and ECC-R-160, respectively). After a degassing process for 2 h at room temperature, the mixture was polymerized in an oven by a curing cycle of 1 h at 80 °C, followed by 20 min at 120 °C and 1 h at 180 °C. To perform this curing cycle, the samples were placed in the oven for the first cure step, with the oven temperature at 80 °C. At the end of the cure treatment at 80 °C (1 h), a heating speed ramp was set to go from 80 °C to 120 °C at 10 °C/min. The sample's actual heating rate (verified with a probe) is 4 °C/min. The same thing happened for the transition from 120 °C to 180 °C.

In this paper, for comparison, the Ep sample, corresponding to the cured epoxy matrix, without the presence of the rubber phase, was prepared by mixing the ECC precursor and the hardener MHHPA and following the procedure previously described. Finally, the functionalized epoxy samples with the selected molecules, reported in Figure 2, were obtained by dispersing the self-healing filler in the functionalized precursor ECC-R-160 by ultrasonication process for 30 min at room temperature. The addition of the hardener and the curing cycle followed the same procedure described above. The obtained samples containing DBA, T, and M were labeled Ep-R-160-DBA, Ep-R-160-T, and Ep-R-160-M, respectively.

2.3. Methods

The preparation of the samples to carry out FT-IR spectra and the modality of their acquisition are described in Section S1 (S.M.). This last section also reported information on the thermal and dynamic mechanical analysis of the performed elaborations.

Self-healing efficiency (η) was evaluated using two different approaches. The first one consists of a fracture test performed with a tapered double cantilever beam (TDCB) geometry sample following a protocol established in literature [12], which allows to calculate the value of the self-healing efficiency by Equation (1),

$$\eta = \frac{P_{CH}}{P_{CV}} \times 100 \quad (1)$$

where P_{CH} and P_{CV} are the critical fracture load of the healed and virgin sample, respectively. The specimens were tested by INSTRON mod. 5967 Dynamometer, using a load cell of 30 KN and a 250 $\mu\text{m}/\text{min}$ displacement rate. The dimensions of the tested samples are reported in Figure S1 of Section S1 of the S.M.

In the second approach, DMA tests were used to evaluate auto-repair ability. The self-healing test was carried out with a continuous dynamic flexural deformation, through which the samples, having dimensions 3 mm \times 10 mm \times 35 mm and a V-shaped starter notch (1 mm \times 2 mm), were analyzed by applying a sinusoidal deformation with a maximum amplitude of 0.1% at a frequency of 1 Hz. An impulsive load of about 25 N induced a pre-crack in the sample. The trend of the mechanical modulus with temperature was considered as representative of the evolution of the healing process in the sample. In this case, η was calculated according to Equation (2) [48,63].

$$\eta = \frac{E_H}{E_V} \times 100 \quad (2)$$

where E_H and E_V are the storage modulus of the healed and virgin sample, respectively.

3. Results and Discussion

3.1. Functionalization of the Epoxy Precursor

3.1.1. FT-IR Analysis

FT-IR investigation was performed to evaluate the best conditions to choose in the functionalization procedure. A key role is played by the catalyst triphenylphosphine (PPh_3),

which is necessary to promote the reaction between epoxy groups of the matrix (ECC) and the carboxylic groups of the rubber phase (R), as depicted in the reaction scheme of Figure 3.

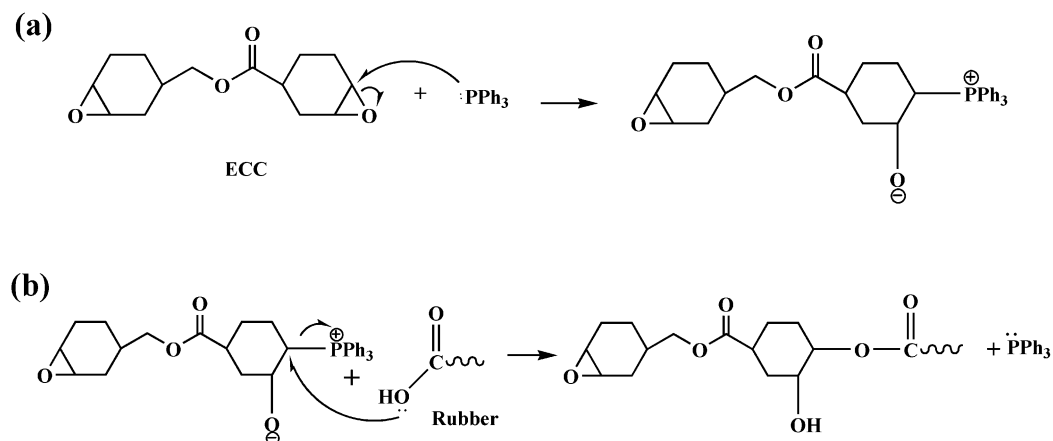


Figure 3. Reaction mechanism supposed for the functionalization of the epoxy precursor: (a) nucleophilic attack of PPh_3 ; (b) reaction of the intermediate with the carboxylic group of the rubber phase.

The presence of PPh_3 is a necessary step to avoid phase separation phenomena between the precursor and the elastomer.

The spectroscopic analyses were carried out on the ECC-R-120 and ECC-R-160 liquid mixtures to investigate the functionalization reaction and the effect of temperature (120 °C and 160 °C, respectively). FTIR spectra of the epoxy precursor ECC, liquid rubber R, and ECC-R blend were compared with the spectrum of the ECC-R-160 blend (see Figures 4 and 5) and the spectrum of the ECC-R-120 blend (see Figures 6 and 7). The liquid blend ECC-R corresponds to the epoxy mixture precursor/elastomer raw before the heat treatments for 15 h. Focusing the attention on Figure 4, in the range between 1650 cm^{-1} and 1850 cm^{-1} (see inset on the left), the spectrum of the rubber phase shows two absorption bands for the ester carbonyl group, as a consequence of the hydrogen bond interactions established among the molecules of the liquid rubber [64]. In particular, the band at 1738 cm^{-1} is ascribed to the free ester carbonyl group, while the band at 1710 cm^{-1} belongs to the H-bonded carbonyl group, involved in the hydrogen bond interactions with the hydroxyl groups of the same rubber molecules. In the same range of wavenumber, the spectrum of the precursor shows the ester $\text{C}=\text{O}$ stretching band, around 1730 cm^{-1} , while the spectrum of the ECC-R blend displays broadband always at 1730 cm^{-1} , which belongs to the carbonyl groups of both the components. In the same region of wavenumber, it is possible to observe the presence of a shoulder peak at 1780 cm^{-1} that could be considered the experimental evidence of the functionalization reaction between the oxirane ring of the epoxy precursor and the carboxylic groups of the rubber phase. This effect is due to the presence of an electron-withdrawing group (hydroxyl group in β position) that can determine the shift of the carbonyl signal to higher values of wavenumber for inductive effect [65]. The peak at 1120 cm^{-1} (see inset on the right of Figure 4), assigned to the $\text{C}-\text{O}$ stretching of the secondary alcohol generated by the opening of the epoxy group during the functionalization reaction, supports the hypothesized mechanism.

Further confirmation of the occurred functionalization is deduced by the results depicted in Figure 5, in the range of wavenumber between 3700 cm^{-1} and 3100 cm^{-1} . ECC-R-160 sample shows an absorption band at 3350 cm^{-1} ascribed to the $-\text{OH}$ groups generated during the reaction. In addition, the absorption band at 3230 cm^{-1} , ascribed to the hydroxyls of the $-\text{COOH}$ group of the R elastomer, disappears after the functionalization reaction.

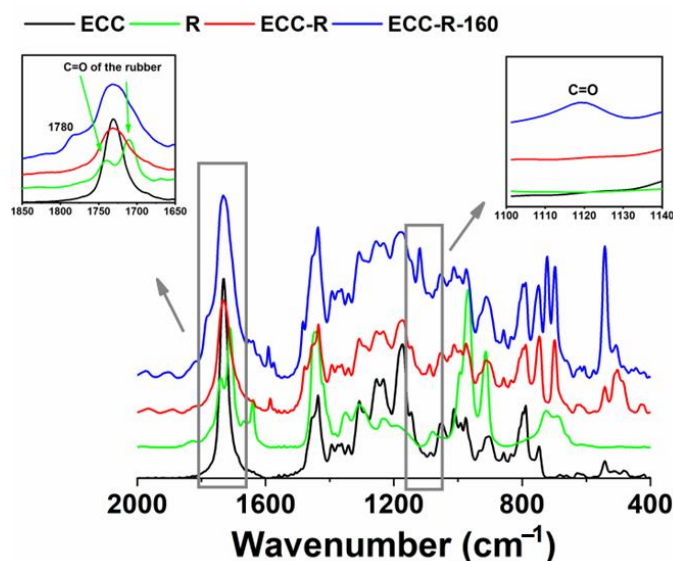


Figure 4. FTIR spectra of the precursor ECC (black curve), the liquid rubber R (green curve), the blend of ECC-R (red curve), and the blend of ECC-R-160 (blue curve), in the range 2000–400 cm^{-1} .

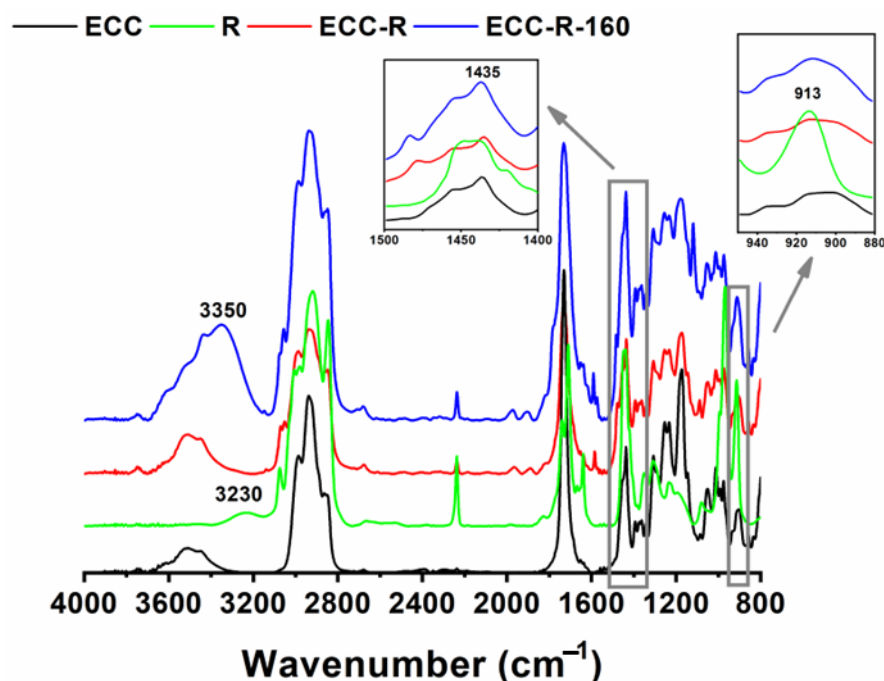


Figure 5. FTIR spectra of the precursor ECC (black curve), the liquid rubber R (green curve), the blend of ECC-R (red curve), and the blend of ECC-R-160 (blue curve), in the range 4000–800 cm^{-1} .

Similar considerations can be made for the ECC-R-120 system, as shown in Figures 6 and 7. Compared to the previous case in the spectrum of the precursor functionalized at 120 °C, the peak around 1780 cm^{-1} is not detectable (see the inset on the left of Figure 6). The reason for this is probably attributable to not very effective functionalization obtained at 120 °C. To evaluate the effectiveness of the functionalization reaction at the two different temperatures (120 °C and 160 °C), a further investigation was carried out in the range between 850 and 950 cm^{-1} , i.e., the area spectrum attributable to the oxirane ring of the precursor. As a consequence of the functionalization reactions, the peak at 913 cm^{-1} , ascribed to the oxirane group of epoxy precursor, decreases in intensity (see the right inset of Figure 5).

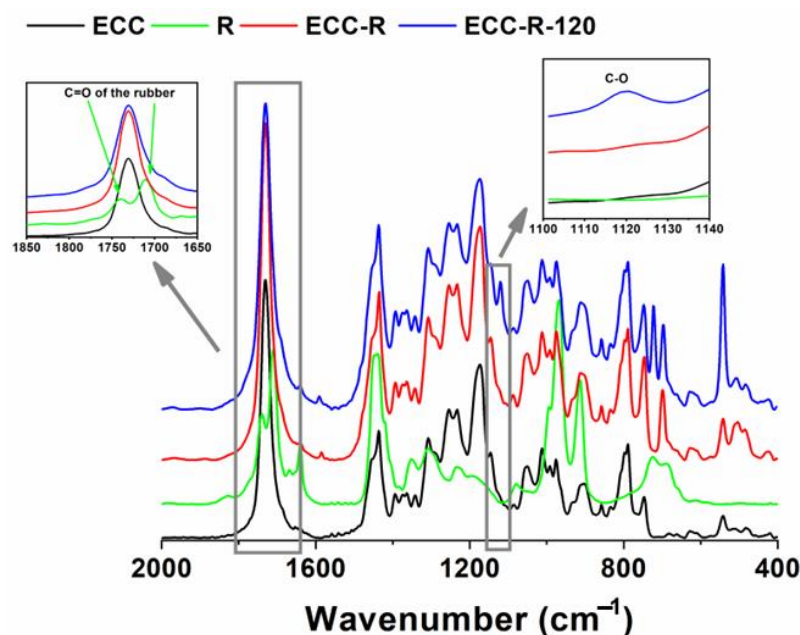


Figure 6. FTIR spectra of the precursor ECC (black curve), the liquid rubber R (green curve), the blend of ECC-R (red curve), and the blend of ECC-R-120 (blue curve), in the range 2000–400 cm^{-1} .

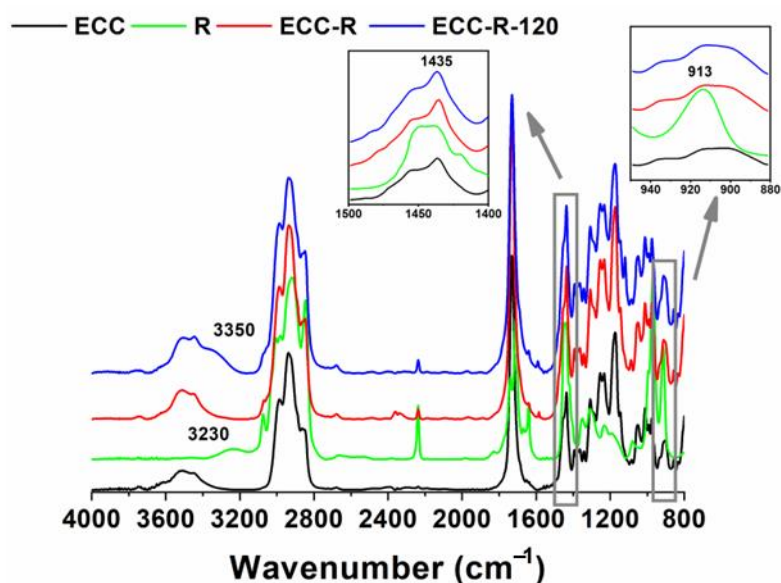


Figure 7. FTIR spectra of the precursor ECC (black curve), the liquid rubber R (green curve), the blend of ECC-R (red curve), and the blend of ECC-R-120 (blue curve), in the range 4000–800 cm^{-1} .

More in particular, the reduction of the peak relative to the oxirane group was evaluated, normalizing the peak at 913 cm^{-1} to the peak at 1435 cm^{-1} associated with the CH_2 stretching of six terms ring, which is assumed chemically unmodified during the reaction [66]. The ratio ($R = A_{\text{peak } 913} / A_{\text{peak } 1435}$) of the subtended areas was evaluated for precursor-liquid rubber system before and after the functionalization process, respectively. An algorithm based on the Levenberg–Marquardt method [67] to separate the individual peaks in the case of unresolved, multicomponent bands, was applied. To reduce the number of adjustable parameters and to ensure the uniqueness of the result, the baseline, the band shape, and the number of components were fixed. The minimum number of components was evaluated by visual in the section based on abrupt changes in the slope of the experimental line shape. The program calculated, by a non-linear curve fitting of data, the

height, the full-width half height (FWHH), and the position of the individual components. The peak function was a mixed Gauss–Lorentz line shape of the form, reported in Equation (3) [68]:

$$f(x) = (1 - L)H \exp \left[-4 \ln(2) \left(\frac{x - x_0}{w} \right)^2 \right] + LH \left[4 \left(\frac{x - x_0}{w} \right)^2 + 1 \right]^{-1} \quad (3)$$

where x_0 = the peak position; H = peak height; w = FWHH; L = fraction of Lorentz character.

The results of this deconvolution procedure for the functionalized precursor at 160 °C, in the above-mentioned ranges of wavenumbers, are shown, respectively, in Figure 8a,b. This procedure was repeated for the systems rubber-precursor before and after the functionalization process at 120 and 160 °C.

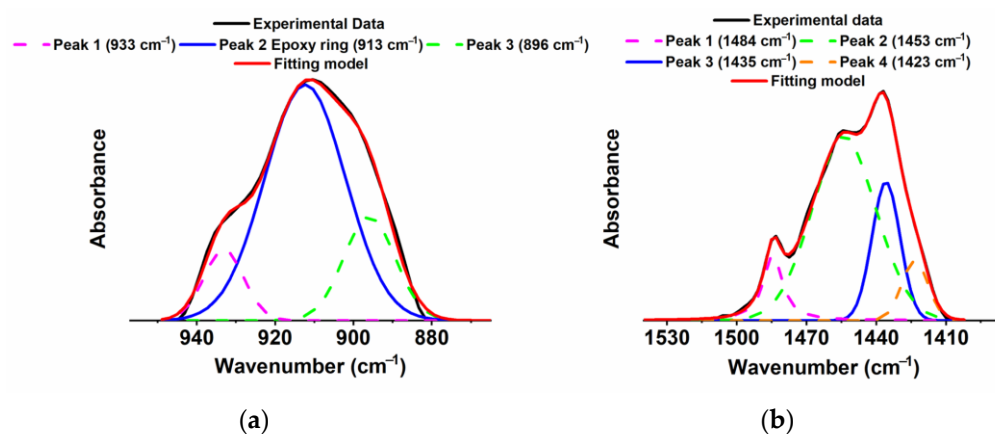


Figure 8. FT-IR spectrum of the ECC-R-160 sample; deconvolution relating to the region of the: (a) epoxy ring; (b) peak at 1435 cm^{-1} associated with the CH_2 stretching.

A reduction of 5.3% and 13.5% was found for ECC-R-120 and ECC-R-160 systems, respectively. This is further proof that the higher temperature value allows for obtaining a greater amount of bond between the carboxyl group of the rubber and the epoxy ring of the precursor, making the precursor functionalization more efficient. The most effective functionalization process affects the resin structure and consequently the thermal and mechanical properties, as described below.

3.1.2. Thermogravimetric Analyses (TGA)

Figure 9 shows the thermogravimetric curves of the ECC, ECC-R-120, and ECC-R-160 samples in air and nitrogen flow.

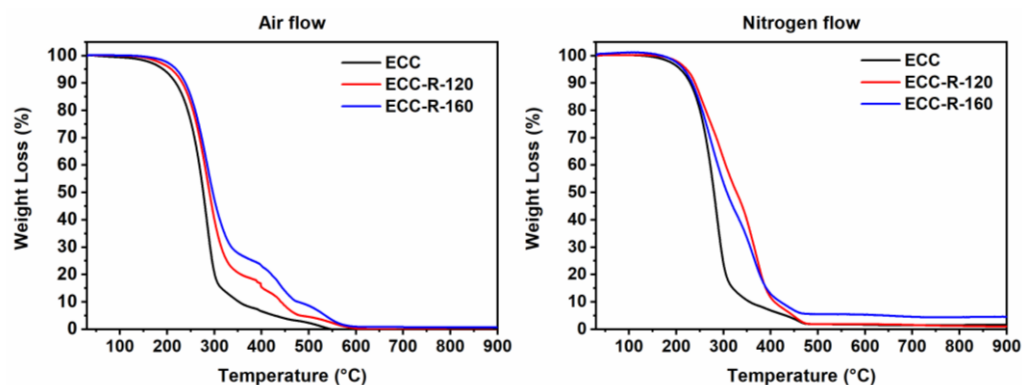


Figure 9. Thermogravimetric curves of ECC sample and the rubber functionalized mixtures ECC-R-120 and ECC-R-160 in air and nitrogen flow.

Comparing the TGA curves of the ECC-R-120 and ECC-R-160 samples with that of sample ECC, it is evident that the thermal stability of the functionalized samples is higher than that of the unfunctionalized resin ECC. Table 2 shows data from TGA analyses performed in air and nitrogen flow for the ECC, ECC-R-120, and ECC-R-160 samples. The initial degradation temperature ($T_{d5\%}$), expressed as temperature corresponding to a weight loss of 5 wt%, presents an increase of about 20 °C and 30 °C for the samples ECC-R-120 and ECC-R-160, respectively. The behaviour in nitrogen flow is the same as observed in air; in this last case, the initial degradation temperature ($T_{d5\%}$) of the samples ECC-R-120 and ECC-R-160 manifests an increase of 13 °C and 7 °C, respectively, with respect to the ECC sample.

Table 2. Data of TGA analyses performed in air and nitrogen flow for ECC, ECC-R-120, and ECC-R-160 samples.

Sample	* $T_{d5\%}$, [°C]
Air flow	
ECC	191.8
ECC-R-120	209.3
ECC-R-160	219.5
Nitrogen flow	
ECC	209.0
ECC-R-120	222.2
ECC-R-160	216.3

* $T_{d5\%}$: temperature corresponding to a weight loss of 5 wt%.

Considering the more reactive environment, the tests performed in air, the functionalized precursor presents a higher thermal stability than the raw precursor.

The functionalization reaction obtained at 160 °C allows for obtaining a modified precursor with greater thermal stability achieving a $T_{d5\%}$ value up to 220 °C.

3.2. Characterization of the Epoxy Resins

3.2.1. Dynamic Mechanical Analysis (DMA)

DMA analyses were carried out on the polymerized samples, with the aim to observe the effect of the functionalization temperature on the mechanical properties of the materials. The tests were performed on the samples Ep, Ep-R-120, and Ep-R-160. DMA investigation was carried out by evaluating the $\tan \delta$ profile and the storage modulus as a function of the temperature. In Figure 10, the DMA curves of the cured functionalized epoxy matrices Ep-R-120 and Ep-R-160 were compared to the curve of the not functionalized epoxy matrix Ep.

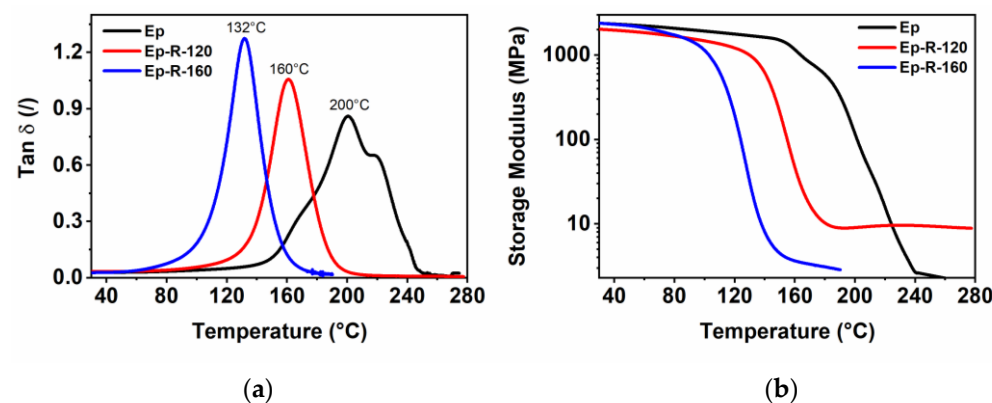


Figure 10. DMA curves: (a) $\tan \delta$ vs. temperature; (b) Storage modulus vs. temperature.

All systems present a storage modulus value (see Figure 10b) higher than 1000 MPa at room temperature and in the wide temperature range of 30 ÷ 100 °C, thus confirming their reliability if employed, for instance, as structural aeronautical parts generally working in the normal operating temperature range. The trend of the not functionalized epoxy matrix (Ep) shows a progressive decrease of modulus up to 150 °C; after that, the principal drop occurs, due to its subsequent attainment of the glass transition temperature (i.e., T_g). The mechanical behavior of this sample, shown in Figure 10a, confirms the glass transition temperature (T_g) value above the 180 °C. The highest peak in the mechanical spectrum, related to the glass transition, (i.e., α transition), is centered at 200 °C. The introduction of the rubber and the different functionalization temperature value affect both storage modulus and $\tan \delta$. The principal drop in the storage modulus is reduced to lower temperature values due to the presence of the functionalized precursor in the resin (see Figure 10b).

One of the big challenges in this work was to improve the resin's dynamic properties and reduce the matrix's rigidity, acting on its phase composition. Therefore, the design of a material containing in a rigid matrix very small domains of rubber phase at higher mobility, finely interpenetrated in the resin, has been considered. A higher mobility is expected of the chains around the elastomeric domains finely distributed in the resin, as highlighted in Section 3.3. Furthermore, DMA analysis evidences a reduction of the rigidity of the matrix (at the macroscopic level). In fact, for the sample which manifests higher healing efficiency (EP-R-160), the peak of $\tan \delta$ vs. temperature opens around 60 °C. It is worth noting that this peak is shifted to a lower temperature range. It involves a temperature range from 60 °C to 180 °C (with a max around 132 °C), where the sample without the rubber phase shows a transition from 140 °C to 250 °C. This is clear evidence of a strong toughening effect exerted by the rubber phase finely distributed in the form of small domains in the resin in a range of temperatures closest to ambient temperature.

The more effective the functionalization reaction of the epoxy precursor, the higher the toughening effect of the elastomer on the polymerized resin. This phenomenon results in a reduction of 40 °C for the Ep-R-120 system and one of 70 °C for the Ep-R-160 system leading the T_g value to 160 °C and 132 °C, respectively (see Figure 10a). These results agree with those obtained through FT-IR and TGA analyses, confirming the efficacy of the precursor functionalization performed at the temperature of 160 °C. To obtain an epoxy resin that shows good auto-repair ability, the composition Ep-R-160 was chosen as the matrix to host self-healing fillers, as the activation of auto-repair mechanism is favored in the presence of higher mobility of the polymeric chains [47,48].

3.2.2. DSC Analyses

DSC investigations were performed to evaluate the influence of the self-healing fillers on the curing process of the functionalized epoxy resin. Figure 11a shows the results of DSC analyses performed on the uncured liquid mixtures.

The presence of the auto-repair agents determines a reduction of the peak temperature (see Table 3) value and a broadening of the peak shape. This phenomenon is more evident in Figure 11b in which the fractional conversion (α) as a function of temperature is shown. The fractional conversion (α) can be expressed as Equation (4):

$$\alpha(T) = \frac{\Delta H_T}{\Delta H_{Tot}} \quad (4)$$

where ΔH_T is the partial heat of reaction at a certain temperature and ΔH_{Tot} is the total heat of reaction. The systems filled with the self-healing agents present a fractional conversion curve shifted at lower temperature and a reduced starting curing temperature value, ($T_{\alpha=0.01}$, temperature value corresponding to $\alpha = 1\%$), as shown in Table 3. DSC curves of the samples EP-R-160, EP-R-160-DBA, EP-R-160-2T, EP-R-160-M, before the curing process (after the functionalization reaction) and after the curing process (dashed curves) have been added in Figure S2 of Section S2 of the S.M.

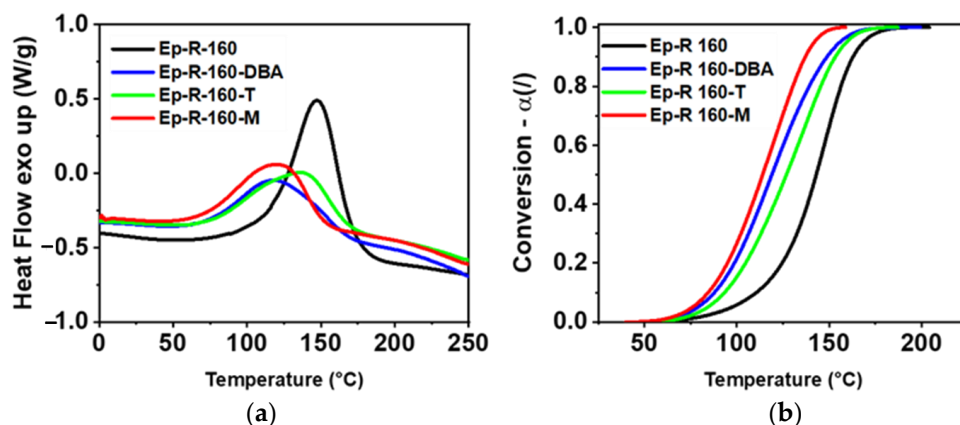


Figure 11. (a) DSC curves of the analyzed samples before the curing process in the oven; (b) Variation of the conversion (α) vs. the temperature.

Table 3. DSC results.

Sample	T_{peak} (°C)	$T_{\alpha=0.01}$ (°C)	ΔH_T (Jg ⁻¹)	ΔH_{Tot} (Jg ⁻¹)	DC (%)
Ep-R-160	147.3	73.1	0	240.75	100.0
Ep-R-160-DBA	117.7	63.3	6.6	121.5	94.6
Ep-R-160-T	135.8	68.1	7.3	138.7	94.7
Ep-R-160-M	120.3	60.6	11.1	123.1	91.0

Table 3 highlights that the presence of the fillers causes, on the one hand, a reduction of curing temperature, on the other, a decrease of the curing degree value, which remains higher than 90%, allowing to the materials to be suitable for structural applications. Usually a small amount of accelerators, such as tertiary amines or imidazoles, are used in the epoxy/anhydride systems to speed up the curing process [69]. In our case, probably, the fillers act as catalysts in the polymerization mechanism. These results could represent an advantage in reducing processing costs and energy savings.

3.2.3. Thermogravimetric Analyses (TGA)

Figure 12 shows the thermogravimetric curves of the rubber functionalized and cured epoxy mixtures Ep-R-160, Ep-R-160-DBA, Ep-R-160-T, and Ep-R-160-M in air and nitrogen flow.

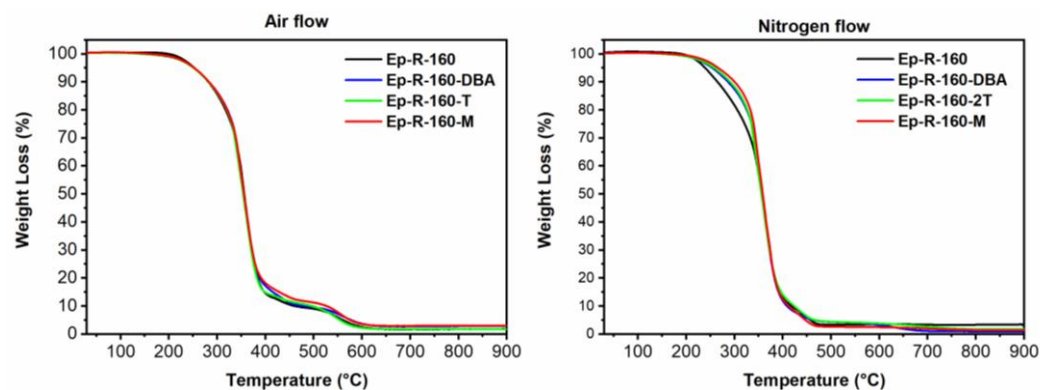


Figure 12. Thermogravimetric curves of the rubber functionalized and cured mixtures Ep-R-160, Ep-R-160-DBA, Ep-R-160-T, and Ep-R-160-M in air and nitrogen flow.

The TGA curves shown in Figure 12, compared with those of Figure 9, clearly evidence that the addition of the hardener agent MHPA determines an increase in the initial degradation temperature ($T_{d5\%}$) of the samples, as expected for samples after the curing

process. For example, for the sample Ep-R-160 (functionalized at a higher temperature), the initial degradation temperature ($T_{d5\%}$) after the curing cycle is about 253 °C in airflow and about 248 °C in nitrogen flow as shown in Table 4. The stability in the thermal degradation is also retained with the dispersion of the self-healing fillers in the formulation.

Table 4. Data of TGA analyses performed in air and nitrogen flow for the sample EP-R-160 and the same sample containing the healing fillers DBA, T, and M.

Sample	* $T_{d5\%}$, [°C]
Air flow	
Ep-R-160	252.8
Ep-R-160-DBA	251.8
Ep-R-160-T	251.1
Ep-R-160-M	252.6
Nitrogen flow	
Ep-R-160	248.4
Ep-R-160-DBA	254.3
Ep-R-160-T	258.2
Ep-R-160-M	266.3

* $T_{d5\%}$: temperature corresponding to a weight loss of 5 wt%.

3.3. Morphological Characterization

Figure 13 shows SEM images of the etched surface of the EP-160-T, EP-160-DBA, and EP-160-M samples. The images give clear information on the size and distribution of the rubber domains in the hosting epoxy matrix. It is worth noting that to better observe the microstructure of the samples, before being analyzed by FESEM, the samples were subjected to an etching process, according to a procedure reported in literature [55].

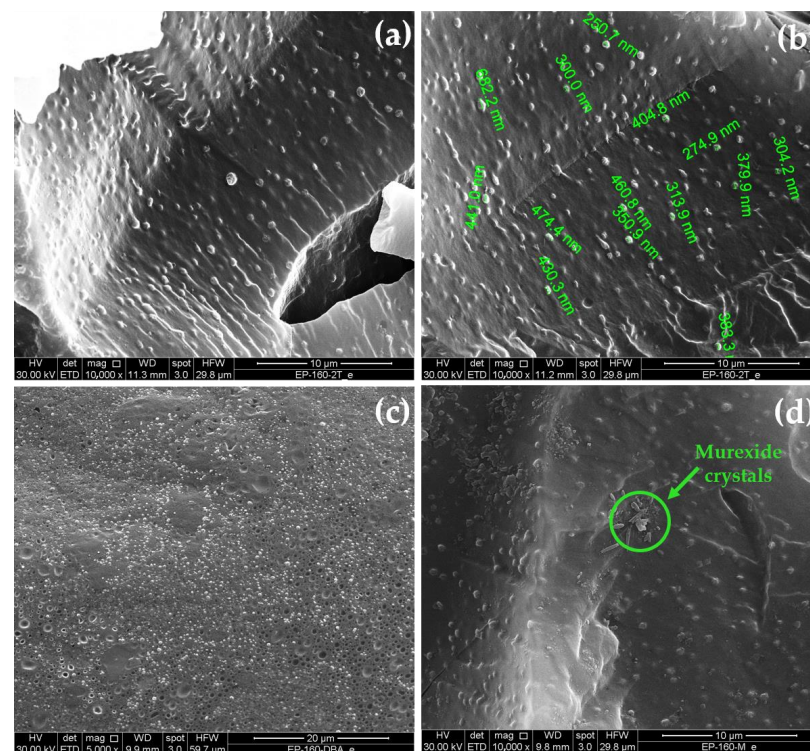


Figure 13. SEM images of the etched surface of: (a,b) the EP-160-T sample; (c) the EP-160-DBA sample; (d) the EP-160-M sample.

Chemical composition and conditions chosen for the functionalization process allow obtaining elastomeric domains of dimensions that do not exceed 500–600 nanometers, as seen in Figure 13a,b for the sample EP-160-T (where also the dimension of rubber domains are indicated on the left image), in Figure 13c for the sample EP-160-DBA, and in Figure 13d for the sample EP-160-M. In the case of M filler, very small crystallites of this component (not completely solubilized in the resin) are also observed in the solidified matrix.

Extensive studies have been carried out on the solubility of self-healing fillers in the components of the epoxy formulation before and after the curing process. Experimental tests and results are reported in Section S3 of the S.M. (see Figure S3-1–S3-4).

It is worth noting that the morphological feature obtained made it possible to maximize the interphase area between the rubber domains.

3.4. Evaluation of Self-Healing Efficiency

Ep-R-160, Ep-R-160-DBA, Ep-R-160-T, and Ep-R-160-M samples were tested to evaluate the self-healing efficiency, as described in Section 2.3 Methods.

The results evaluated with the TDCB geometry at 25 °C are shown in Figure 14. In particular, Figure 14a–c show the behaviour of load as a function of the displacement for the virgin samples Ep-R-160-DBA, Ep-R-160-T, and Ep-R-160-M (continuous line) and the same healed samples (dashed line). Figure 14d depicts the histogram of the values of healing efficiency, calculated by Equation (1), using the values of P_{CV} and P_{CH} , reported in Table 5. The introduction of the self-healing fillers causes a recovery of mechanical properties. The healing efficiency value is higher than 69% for all fillers. The highest value was detected for the sample with DBA, for which a value of 88% was found. Statistically, the tests performed on different samples with the same composition and treatments showed values with standard deviations of around 5%

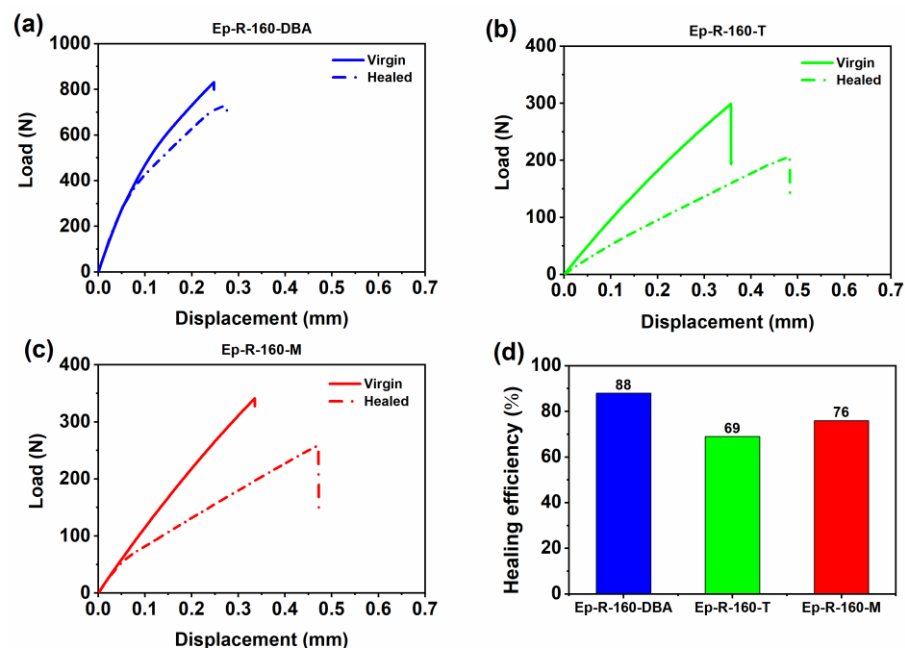


Figure 14. Load-Displacement curves for the samples (a) Ep-R-160-DBA; (b) Ep-R-160-T; (c) Ep-R-160-M; and (d) histogram illustrating the healing efficiency values.

Table 5. Critical fracture loads values of the analyzed samples.

Sample	P_{CV} (N)	P_{CH} (N)
Ep-R-160-DBA	831	730
Ep-R-160-T	299	207
Ep-R-160-M	341	259

Most likely, the high healing efficiency values are due to polar groups in the self-healing fillers, such as O-H, N-H, and C=O functional groups. These groups act as hydrogen bond donors or acceptors with the polar groups of the functionalized epoxy-precursor, establishing cumulative effects of the attractive reversible interactions. The attractive reversible interactions are probably established much more effectively in the higher mobility domains of the polymeric chains, therefore, at the interface between the rubbery domains and the matrix resin (where the degree of crosslinking is reduced).

Notably, the peculiar morphology of these samples, with rubber domains of dimensions in the order of a few hundred nanometres (see Figure 13), contributes to increasing the areas at reduced crosslinking density.

An example of possible interactions based on reversible hydrogen bonds is shown in Figure 15, which depicts the H-bond interactions built between the hydroxyl groups, acting as H-bond donor sites, of the cured epoxy resin and the carbonyl groups, acting as H-bond acceptor sites, of the DBA filler. The resulting supramolecular network activates self-healing mechanisms in the formulated materials.

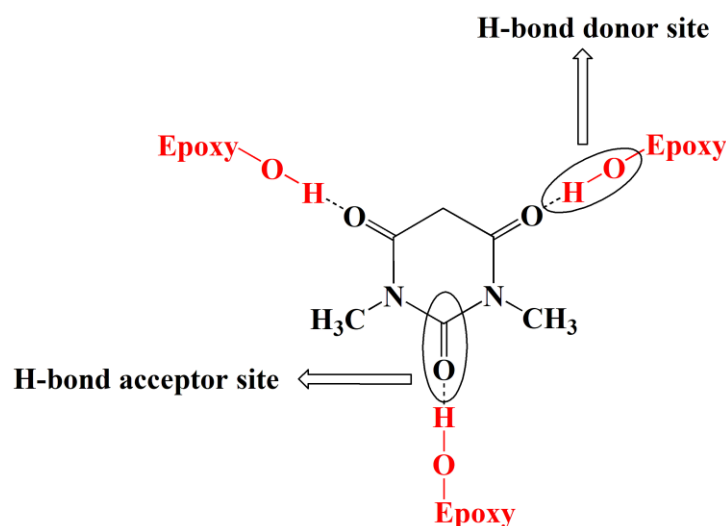


Figure 15. Picture illustrating the H-bond interactions between the hydroxyl groups of the epoxy resin (red highlighted) and the carbonyl groups of the DBA filler.

Hydrogen bonds are widely recognized to activate self-healing processes [70–72], it has mostly been applied in rubbery matrices [47,73–75]. In our samples, we have small rubber domains distributed throughout the whole sample. The employment of reversible hydrogen bonds in epoxy resins has only been reported in specially modified systems through the addition of hydrogen bonding moieties such as ureido- pyrimidinone (UPy) [76,77], barbiturate and thymine functionalized MWCNTs [48], and amide motifs [78]. Reference [48] refers to our previously published paper on self-healing resins. These papers describe self-healing resins, where barbiturate and thymine functionalized MWCNTs were embedded in a rubber-toughened epoxy formulation. The groups with hydrogen donor or acceptor sites lead to reversible MWCNTs-bridges through the matrix due to strong, attractive interactions between the rubber phase, finely dispersed in the matrix, and MWCNT walls. Healing efficiencies higher than 50% have been found for both functional groups. Dynamic mechanical analysis (DMA) evidenced an enhancement in epoxy chain movements due to the rubber phase's micro/nanodomains, enabling self-healing behavior by recovering the critical fracture load. In this paper, molecules capable of establishing strong cumulative effects due to hydrogen bonds have been dispersed in the toughened thermosetting matrix.

The authors demonstrate that the effect of the functionalization temperature should not be underestimated to evaluate the healing ability of the materials. Figure S4 of Section S4 of S.M. shows the results of self-healing tests carried out for the samples Ep-R-120 and

Ep-R-160 loaded with the DBA filler (Ep-R-120-DBA and Ep-R-160-DBA, respectively). The comparison between Ep-R-120-DBA and Ep-R-160-DBA shows that the functionalization temperature of 160 °C allows an increase in the self-healing efficiency, as expected considering the DMA results in Figure 11, where a lower value of T_g is observed for the sample functionalized at 160 °C.

DMA results of this last sample including the self-healing fillers (see Figure 16) show that the T_g values of the complete formulations are lower than the same sample without filler (132 °C, see Figure 11) of about 10 °C for Ep-R-160-DBA, Ep-R-160-T, and Ep-R-160-M.

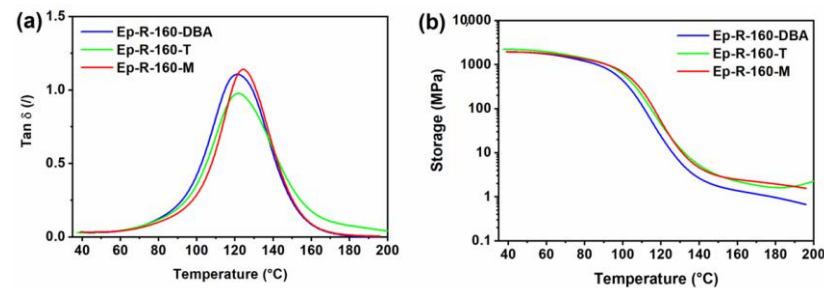


Figure 16. DMA curves: (a) Tan δ vs. temperature; (b) Storage modulus vs. temperature of the samples Ep-R-160-DBA, Ep-R-160-T, and Ep-R-160-M.

The modulus drop (see Figure 16b) is slightly anticipated for the sample containing the DBA filler for which the highest healing efficiency value is recorded.

4. Conclusions

In this study, a bifunctional epoxy precursor was functionalized with a rubber phase. Then, self-healing molecules were added to the rubber-toughened bifunctional epoxy resin to confer it auto-repair function. The functionalization process allows obtaining elastomeric domains not exceeding 500–600 nanometers. After the curing cycle of the formulated self-healing samples, the effect of the temperature of epoxy precursor functionalization on the properties of the samples was evaluated in terms of self-healing efficiency, DMA, and TGA. It was found that the higher functionalization temperature of 160 °C can better promote the reaction between the rubber phase and the epoxy precursor during the functionalization process. The more efficient interactions affect the resin structure and its thermal and mechanical properties. Self-healing efficiency analysis highlights the crucial role of functionalization temperature in increasing self-healing ability. Samples functionalized at 160 °C manifest healing efficiency higher than 69%. The highest value (88%) was detected for the sample with DBA filler. The healing efficiency of the same sample functionalized at 120 °C decreases to 52%. Results from DMA evidence that a lower value of T_g (observed for the sample functionalized at the higher temperature of 160 °C) allows for obtaining the highest healing efficiency. Thermal stability in air higher than 250 °C was observed for all formulated samples.

Supplementary Materials: The following supporting information can be downloaded at <https://www.mdpi.com/article/10.3390/aerospace10050476/s1>: Figure S1: Dimensions of the TDCB geometry specimen (on the left); EP-R-160 sample located in the INSTRON instrument (on the right). Numerical values of the lengths are expressed in mm; Figure S2: DSC curves of the samples EP-R-160, EP-R-160-DBA, EP-R-160-T, EP-R-160-M, before the curing process (after the functionalization reaction) and after the curing process; Figure S3-1: Photos of the self-healing fillers after incorporation into the Gurit precursor ECC at room temperature; Figure S3-2: Photos of the self-healing fillers before incorporation into the Gurit hardener MHPA; Figure S3-3: Photos of the self-healing fillers after incorporation into the Gurit hardener MHPA; Figure S3-4: Visualization of the complete solubilization of the self-healing fillers in the Gurit hardener MHPA; Figure S4: (a) Load-Displacement curves for the sample Ep-R-120-DBA; and (b) histogram illustrating the healing efficiency values for the samples Ep-R-120-DBA and EP-R-160-DBA.

Author Contributions: Conceptualization, methodology, supervision, project administration, writing—original draft, writing—review and editing L.G.; Formal analysis; investigation M.R., C.N., R.L. and A.S.; Resources M.C.; Conceptualization, formal analysis, data curation, writing—original draft, investigation, writing—review and editing E.C. and L.V. All authors have read and agreed to the published version of the manuscript.

Funding: The research leading to these results was funded by the European Union’s Seventh Framework Programme for Research, Technological Development and Demonstration, under Grant Agreement N 313978.

Data Availability Statement: Not applicable.

Conflicts of Interest: The authors declare no conflict of interest.

References

1. Fugolin, A.P.; Pfeifer, C.S. Engineering a new generation of thermoset self-healing polymers based on intrinsic approaches. *JADA Found. Sci.* **2022**, *1*, 100014. [[CrossRef](#)]
2. Ha, Y.-M.; Seo, H.C.; Kim, Y.-O.; Khil, M.-S.; Cho, J.W.; Lee, J.-S.; Jung, Y.C. Effects of hard segment of polyurethane with disulfide bonds on shape memory and self-healing ability. *Macromol. Res.* **2020**, *28*, 234–240. [[CrossRef](#)]
3. Lee, W.-J.; Oh, H.-G.; Cha, S.-H. A brief review of self-healing polyurethane based on dynamic chemistry. *Macromol. Res.* **2021**, *29*, 649–664. [[CrossRef](#)]
4. Li, B.; Cao, P.-F.; Saito, T.; Sokolov, A.P. Intrinsically Self-Healing Polymers: From Mechanistic Insight to Current Challenges. *Chem. Rev.* **2022**, *132*, 701–735. [[CrossRef](#)] [[PubMed](#)]
5. Montero de Espinosa, L.; Meesorn, W.; Moatsou, D.; Weder, C. Bioinspired polymer systems with stimuli-responsive mechanical properties. *Chem. Rev.* **2017**, *117*, 12851–12892. [[CrossRef](#)] [[PubMed](#)]
6. Nik Md Noordin Kahar, N.N.F.; Osman, A.F.; Alosime, E.; Arsat, N.; Mohammad Azman, N.A.; Syamsir, A.; Itam, Z.; Abdul Hamid, Z.A. The versatility of polymeric materials as self-healing agents for various types of applications: A review. *Polymers* **2021**, *13*, 1194. [[CrossRef](#)] [[PubMed](#)]
7. Thakur, V.K.; Kessler, M.R. Self-healing polymer nanocomposite materials: A review. *Polymer* **2015**, *69*, 369–383. [[CrossRef](#)]
8. Utrera-Barrios, S.; Verdejo, R.; López-Manchado, M.A.; Santana, M.H. Evolution of self-healing elastomers, from extrinsic to combined intrinsic mechanisms: A review. *Mater. Horiz.* **2020**, *7*, 2882–2902. [[CrossRef](#)]
9. Wemyss, A.M.; Bowen, C.; Plesse, C.; Vancaeyzeele, C.; Nguyen, G.T.; Vidal, F.; Wan, C. Dynamic crosslinked rubbers for a green future: A material perspective. *Mater. Sci. Eng. R Rep.* **2020**, *141*, 100561. [[CrossRef](#)]
10. Zhu, M.; Liu, J.; Gan, L.; Long, M. Research progress in bio-based self-healing materials. *Eur. Polym. J.* **2020**, *129*, 109651. [[CrossRef](#)]
11. Blaiszik, B.J.; Kramer, S.L.; Olugebefola, S.C.; Moore, J.S.; Sottos, N.R.; White, S.R. Self-healing polymers and composites. *Annu. Rev. Mater. Res.* **2010**, *40*, 179–211. [[CrossRef](#)]
12. Brown, E.N.; Sottos, N.R.; White, S.R. Fracture testing of a self-healing polymer composite. *Exp. Mech.* **2002**, *42*, 372–379. [[CrossRef](#)]
13. Guadagno, L.; Longo, P.; Raimondo, M.; Naddeo, C.; Mariconda, A.; Sorrentino, A.; Vittoria, V.; Iannuzzo, G.; Russo, S. Cure behavior and mechanical properties of structural self-healing epoxy resins. *J. Polym. Sci. Part B Polym. Phys.* **2010**, *48*, 2413–2423. [[CrossRef](#)]
14. Raimondo, M.; De Nicola, F.; Volponi, R.; Binder, W.; Michael, P.; Russo, S.; Guadagno, L. Self-repairing CFRPs targeted towards structural aerospace applications. *Int. J. Struct. Integr.* **2016**, *7*, 656–670. [[CrossRef](#)]
15. White, S.R.; Sottos, N.R.; Geubelle, P.H.; Moore, J.S.; Kessler, M.R.; Sriram, S.; Brown, E.N.; Viswanathan, S. Autonomic healing of polymer composites. *Nature* **2001**, *409*, 794–797. [[CrossRef](#)]
16. Jin, H.; Miller, G.M.; Pety, S.J.; Griffin, A.S.; Stradley, D.S.; Roach, D.; Sottos, N.R.; White, S.R. Fracture behavior of a self-healing, toughened epoxy adhesive. *Int. J. Adhes. Adhes.* **2013**, *44*, 157–165. [[CrossRef](#)]
17. Dry, C. Procedures developed for self-repair of polymer matrix composite materials. *Compos. Struct.* **1996**, *35*, 263–269. [[CrossRef](#)]
18. Dry, C.M.; Sottos, N.R. Passive smart self-repair in polymer matrix composite materials. In *Smart Structures and Materials 1993: Smart Materials*; SPIE: Bellingham, WA, USA, 1993; pp. 438–444.
19. Williams, H.; Trask, R.; Knights, A.; Williams, E.; Bond, A.I. Biomimetic reliability strategies for self-healing vascular networks in engineering materials. *J. R. Soc. Interface* **2008**, *5*, 735–747. [[CrossRef](#)]
20. Williams, H.; Trask, R.; Weaver, P.; Bond, I. Minimum mass vascular networks in multifunctional materials. *J. R. Soc. Interface* **2008**, *5*, 55–65. [[CrossRef](#)]
21. Goyal, M.; Agarwal, S.N.; Bhatnagar, N. A review on self-healing polymers for applications in spacecraft and construction of roads. *J. Appl. Polym. Sci.* **2022**, *139*, e52816. [[CrossRef](#)]
22. Chen, X.; Dam, M.A.; Ono, K.; Mal, A.; Shen, H.; Nutt, S.R.; Sheran, K.; Wudl, F. A thermally re-mendable cross-linked polymeric material. *Science* **2002**, *295*, 1698–1702. [[CrossRef](#)] [[PubMed](#)]

23. Chen, X.; Wudl, F.; Mal, A.K.; Shen, H.; Nutt, S.R. New thermally remendable highly cross-linked polymeric materials. *Macromolecules* **2003**, *36*, 1802–1807. [[CrossRef](#)]
24. Ehrhardt, D.; Mangialetto, J.; Bertouille, J.; Van Durme, K.; Van Mele, B.; Van den Brande, N. Self-healing in mobility-restricted conditions maintaining mechanical robustness: Furan–maleimide diels–alder cycloadditions in polymer networks for ambient applications. *Polymers* **2020**, *12*, 2543. [[CrossRef](#)] [[PubMed](#)]
25. Jung, S.; Oh, J.K. Well-defined methacrylate copolymer having reactive maleimide pendants for fabrication of thermally-labile crosslinked networks with robust self-healing. *Mater. Today Commun.* **2017**, *13*, 241–247. [[CrossRef](#)]
26. Murphy, E.B.; Bolanos, E.; Schaffner-Hamann, C.; Wudl, F.; Nutt, S.R.; Auad, M.L. Synthesis and characterization of a single-component thermally remendable polymer network: Staudinger and Stille revisited. *Macromolecules* **2008**, *41*, 5203–5209. [[CrossRef](#)]
27. Park, J.S.; Kim, H.S.; Hahn, H.T. Healing behavior of a matrix crack on a carbon fiber/mendomer composite. *Compos. Sci. Technol.* **2009**, *69*, 1082–1087. [[CrossRef](#)]
28. Park, J.S.; Takahashi, K.; Guo, Z.; Wang, Y.; Bolanos, E.; Hamann-Schaffner, C.; Murphy, E.; Wudl, F.; Hahn, H.T. Towards development of a self-healing composite using a mendable polymer and resistive heating. *J. Compos. Mater.* **2008**, *42*, 2869–2881. [[CrossRef](#)]
29. Peterson, A.M.; Jensen, R.E.; Palmese, G.R. Reversibly cross-linked polymer gels as healing agents for epoxy– amine thermosets. *ACS Appl. Mater. Interfaces* **2009**, *1*, 992–995. [[CrossRef](#)]
30. Peterson, A.M.; Jensen, R.E.; Palmese, G.R. Room-temperature healing of a thermosetting polymer using the Diels–Alder reaction. *ACS Appl. Mater. Interfaces* **2010**, *2*, 1141–1149. [[CrossRef](#)]
31. Plaisted, T.A.; Nemat-Nasser, S. Quantitative evaluation of fracture, healing and re-healing of a reversibly cross-linked polymer. *Acta Mater.* **2007**, *55*, 5684–5696. [[CrossRef](#)]
32. Pratama, P.A.; Sharifi, M.; Peterson, A.M.; Palmese, G.R. Room temperature self-healing thermoset based on the Diels–Alder reaction. *ACS Appl. Mater. Interfaces* **2013**, *5*, 12425–12431. [[CrossRef](#)] [[PubMed](#)]
33. Wang, D.; Chen, S.; Zhao, J.; Zhang, Z. Synthesis and characterization of self-healing cross-linked non-isocyanate polyurethanes based on Diels–Alder reaction with unsaturated polyester. *Mater. Today Commun.* **2020**, *23*, 101138. [[CrossRef](#)]
34. Hayes, S.; Jones, F.; Marshiya, K.; Zhang, W. A self-healing thermosetting composite material. *Compos. Part A Appl. Sci. Manuf.* **2007**, *38*, 1116–1120. [[CrossRef](#)]
35. Luo, X.; Ou, R.; Eberly, D.E.; Singhal, A.; Viratyaporn, W.; Mather, P.T. A thermoplastic/thermoset blend exhibiting thermal mending and reversible adhesion. *ACS Appl. Mater. Interfaces* **2009**, *1*, 612–620. [[CrossRef](#)]
36. Kalista, S.J., Jr.; Ward, T.C. Thermal characteristics of the self-healing response in poly (ethylene-co-methacrylic acid) copolymers. *J. R. Soc. Interface* **2007**, *4*, 405–411. [[CrossRef](#)]
37. Kalista, S.J., Jr.; Ward, T.C.; Oyetunji, Z. Self-healing of poly (ethylene-co-methacrylic acid) copolymers following projectile puncture. *Mech. Adv. Mater. Struct.* **2007**, *14*, 391–397. [[CrossRef](#)]
38. Varley, R.J.; van der Zwaag, S. Towards an understanding of thermally activated self-healing of an ionomer system during ballistic penetration. *Acta Mater.* **2008**, *56*, 5737–5750. [[CrossRef](#)]
39. Varley, R.J.; van der Zwaag, S. Development of a quasi-static test method to investigate the origin of self-healing in ionomers under ballistic conditions. *Polym. Test.* **2008**, *27*, 11–19. [[CrossRef](#)]
40. McGarel, O.J.; Wool, R.P. Craze growth and healing in polystyrene. *J. Polym. Sci. Part B Polym. Phys.* **1987**, *25*, 2541–2560. [[CrossRef](#)]
41. O'Connor, K.; Wool, R. Optical studies of void formation and healing in styrene-isoprene-styrene block copolymers. *J. Appl. Phys.* **1980**, *51*, 5075–5079. [[CrossRef](#)]
42. Wool, R.; O'Connor, K. A theory crack healing in polymers. *J. Appl. Phys.* **1981**, *52*, 5953–5963. [[CrossRef](#)]
43. Cordier, P.; Tournilhac, F.; Soulié-Ziakovic, C.; Leibler, L. Self-healing and thermoreversible rubber from supramolecular assembly. *Nature* **2008**, *451*, 977–980. [[CrossRef](#)]
44. Montarnal, D.; Tournilhac, F.; Hidalgo, M.; Couturier, J.-L.; Leibler, L. Versatile one-pot synthesis of supramolecular plastics and self-healing rubbers. *J. Am. Chem. Soc.* **2009**, *131*, 7966–7967. [[CrossRef](#)] [[PubMed](#)]
45. Longo, P.; Mariconda, A.; Calabrese, E.; Raimondo, M.; Naddeo, C.; Vertuccio, L.; Russo, S.; Iannuzzo, G.; Guadagno, L. Development of a new stable ruthenium initiator suitably designed for self-repairing applications in high reactive environments. *J. Ind. Eng. Chem.* **2017**, *54*, 234–251. [[CrossRef](#)]
46. Zhang, F.; Zhang, L.; Yaseen, M.; Huang, K. A review on the self-healing ability of epoxy polymers. *J. Appl. Polym. Sci.* **2021**, *138*, 50260. [[CrossRef](#)]
47. Guadagno, L.; Raimondo, M.; Naddeo, C.; Vertuccio, L.; Russo, S.; Iannuzzo, G.; Calabrese, E. Rheological, Thermal and Mechanical Characterization of Toughened Self-Healing Supramolecular Resins, Based on Hydrogen Bonding. *Nanomaterials* **2022**, *12*, 4322. [[CrossRef](#)]
48. Guadagno, L.; Vertuccio, L.; Naddeo, C.; Calabrese, E.; Barra, G.; Raimondo, M.; Sorrentino, A.; Binder, W.H.; Michael, P.; Rana, S. Reversible self-healing carbon-based nanocomposites for structural applications. *Polymers* **2019**, *11*, 903. [[CrossRef](#)]
49. Ricciardi, M.; Papa, I.; Langella, A.; Langella, T.; Lopresto, V.; Antonucci, V. Mechanical properties of glass fibre composites based on nitrile rubber toughened modified epoxy resin. *Compos. Part B Eng.* **2018**, *139*, 259–267. [[CrossRef](#)]

50. Karger-Kocsis, J.; Friedrich, K. Fatigue crack propagation and related failure in modified, anhydride-cured epoxy resins. *Colloid Polym. Sci.* **1992**, *270*, 549–562. [[CrossRef](#)]
51. Karger-Kocsis, J.; Friedrich, K. Microstructure-related fracture toughness and fatigue crack growth behaviour in toughened, anhydride-cured epoxy resins. *Compos. Sci. Technol.* **1993**, *48*, 263–272. [[CrossRef](#)]
52. Ramos, V.D.; Da Costa, H.M.; Soares, V.L.; Nascimento, R.S. Modification of epoxy resin: A comparison of different types of elastomer. *Polym. Test.* **2005**, *24*, 387–394. [[CrossRef](#)]
53. Guadagno, L.; Vertuccio, L.; Foglia, F.; Raimondo, M.; Barra, G.; Sorrentino, A.; Pantani, R.; Calabrese, E. Flexible eco-friendly multilayer film heaters. *Compos. Part B Eng.* **2021**, *224*, 109208. [[CrossRef](#)]
54. Vertuccio, L.; Foglia, F.; Pantani, R.; Romero-Sánchez, M.; Calderón, B.; Guadagno, L. Carbon nanotubes and expanded graphite based bulk nanocomposites for de-icing applications. *Compos. Part B Eng.* **2021**, *207*, 108583. [[CrossRef](#)]
55. Guadagno, L.; Aliberti, F.; Longo, R.; Raimondo, M.; Pantani, R.; Sorrentino, A.; Catauro, M.; Vertuccio, L. Electrical anisotropy controlled heating of acrylonitrile butadiene styrene 3D printed parts. *Mater. Des.* **2023**, *225*, 111507. [[CrossRef](#)]
56. Böger, L.; Wichmann, M.H.; Meyer, L.O.; Schulte, K. Load and health monitoring in glass fibre reinforced composites with an electrically conductive nanocomposite epoxy matrix. *Compos. Sci. Technol.* **2008**, *68*, 1886–1894. [[CrossRef](#)]
57. Hu, N.; Itoi, T.; Akagi, T.; Kojima, T.; Xue, J.; Yan, C.; Atobe, S.; Fukunaga, H.; Yuan, W.; Ning, H. Ultrasensitive strain sensors made from metal-coated carbon nanofiller/epoxy composites. *Carbon* **2013**, *51*, 202–212. [[CrossRef](#)]
58. Guadagno, L.; Longo, R.; Aliberti, F.; Lamberti, P.; Tucci, V.; Pantani, R.; Spinelli, G.; Catauro, M.; Vertuccio, L. Role of MWCNTs Loading in Designing Self-Sensing and Self-Heating Structural Elements. *Nanomaterials* **2023**, *13*, 495. [[CrossRef](#)]
59. Prolongo, S.; Moriche, R.; Del Rosario, G.; Jiménez-Suárez, A.; Prolongo, M.; Ureña, A. Joule effect self-heating of epoxy composites reinforced with graphitic nanofillers. *J. Polym. Res.* **2016**, *23*, 189. [[CrossRef](#)]
60. Yang, P.; Ghosh, S.; Xia, T.; Wang, J.; Bissett, M.A.; Kinloch, I.A.; Barg, S. Joule Heating and mechanical properties of epoxy/graphene based aerogel composite. *Compos. Sci. Technol.* **2022**, *218*, 109199. [[CrossRef](#)]
61. Guadagno, L.; Sorrentino, A.; Delprat, P.; Vertuccio, L. Design of multifunctional composites: New strategy to save energy and improve mechanical performance. *Nanomaterials* **2020**, *10*, 2285. [[CrossRef](#)]
62. Vertuccio, L.; Guadagno, L.; Spinelli, G.; Russo, S.; Iannuzzo, G. Effect of carbon nanotube and functionalized liquid rubber on mechanical and electrical properties of epoxy adhesives for aircraft structures. *Compos. Part B Eng.* **2017**, *129*, 1–10. [[CrossRef](#)]
63. Guadagno, L.; Vertuccio, L.; Barra, G.; Naddeo, C.; Sorrentino, A.; Lavorgna, M.; Raimondo, M.; Calabrese, E. Eco-friendly polymer nanocomposites designed for self-healing applications. *Polymer* **2021**, *223*, 123718. [[CrossRef](#)]
64. Coleman, M.M.; Skrovanek, D.J.; Hu, J.; Painter, P.C. Hydrogen bonding in polymer blends. 1. FTIR studies of urethane-ether blends. *Macromolecules* **1988**, *21*, 59–65. [[CrossRef](#)]
65. Neuvonen, H.; Neuvonen, K. Correlation analysis of carbonyl carbon ¹³C NMR chemical shifts, IR absorption frequencies and rate coefficients of nucleophilic acyl substitutions. A novel explanation for the substituent dependence of reactivity. *J. Chem. Soc. Perkin Trans. 2* **1999**, *7*, 1497–1502. [[CrossRef](#)]
66. Li, G.; Xu, M.; Larsen, S.; Grassian, V. Photooxidation of cyclohexane and cyclohexene in BaY. *J. Mol. Catal. A Chem.* **2003**, *194*, 169–180. [[CrossRef](#)]
67. Marquardt, D.W. An algorithm for least-squares estimation of nonlinear parameters. *J. Soc. Ind. Appl. Math.* **1963**, *11*, 431–441. [[CrossRef](#)]
68. Maddams, W. The scope and limitations of curve fitting. *Appl. Spectrosc.* **1980**, *34*, 245–267. [[CrossRef](#)]
69. Mark, H.F. *Encyclopedia of Polymer Science and Technology*, 15 Volume Set; Wiley: New York, NY, USA, 2014; Volume 14.
70. Bouteiller, L. Assembly via hydrogen bonds of low molar mass compounds into supramolecular polymers. *Hydrog. Bond. Polym.* **2007**, *207*, 79–112.
71. García, S.; Fischer, H.; Van Der Zwaag, S. A critical appraisal of the potential of self healing polymeric coatings. *Prog. Org. Coat.* **2011**, *72*, 211–221. [[CrossRef](#)]
72. Peñas-Caballero, M.; Santana, M.H.; Verdejo, R.; Lopez-Manchado, M.A. Measuring self-healing in epoxy matrices: The need for standard conditions. *React. Funct. Polym.* **2021**, *161*, 104847. [[CrossRef](#)]
73. Cao, L.; Yuan, D.; Xu, C.; Chen, Y. Biobased, self-healable, high strength rubber with tunicate cellulose nanocrystals. *Nanoscale* **2017**, *9*, 15696–15706. [[CrossRef](#)] [[PubMed](#)]
74. Thangavel, G.; Tan, M.W.M.; Lee, P.S. Advances in self-healing supramolecular soft materials and nanocomposites. *Nano Converg.* **2019**, *6*, 29. [[CrossRef](#)] [[PubMed](#)]
75. Utrera-Barrios, S.; Hernández Santana, M.; Verdejo, R.; López-Manchado, M.A. Design of rubber composites with autonomous self-healing capability. *ACS Omega* **2020**, *5*, 1902–1910. [[CrossRef](#)] [[PubMed](#)]
76. Kostopoulos, V.; Kotrotsos, A.; Tsantzalis, S.; Tsokanas, P.; Loutas, T.; Bosman, A. Toughening and healing of continuous fibre reinforced composites by supramolecular polymers. *Compos. Sci. Technol.* **2016**, *128*, 84–93. [[CrossRef](#)]

77. Zhang, P.; Kan, L.; Zhang, X.; Li, R.; Qiu, C.; Ma, N.; Wei, H. Supramolecularly toughened and elastic epoxy resins by grafting 2-ureido-4 [1H]-pyrimidone moieties on the side chain. *Eur. Polym. J.* **2019**, *116*, 126–133. [[CrossRef](#)]
78. Villani, M.; Deshmukh, Y.S.; Camlibel, C.; Esteves, A.C.C. Superior relaxation of stresses and self-healing behavior of epoxy-amine coatings. *RSC Adv.* **2016**, *6*, 245–259. [[CrossRef](#)]

Disclaimer/Publisher’s Note: The statements, opinions and data contained in all publications are solely those of the individual author(s) and contributor(s) and not of MDPI and/or the editor(s). MDPI and/or the editor(s) disclaim responsibility for any injury to people or property resulting from any ideas, methods, instructions or products referred to in the content.